

Refractive index retrieval by combining the contrast transfer function and SART in X-ray in-line phase tomography

LORIANE WEBER¹, MAX LANGER¹, FRANÇOISE PEYRIN¹

¹ Université de Lyon, CREATIS, CNRS UMR 5220 ; INSERM U1044 ; INSA-Lyon ; Université Lyon 1
ESRF - The European Synchrotron, 71 Avenue des Martyrs, CS40220, 38043 Grenoble Cedex 9

¹loriane.weber@esrf.fr, max.langer@esrf.fr, peyrin@esrf.fr

Résumé - Ce travail présente un algorithme itératif innovant pour la reconstruction en micro-tomographie X de phase par rayonnement synchrotron. La technique d'acquisition est basée sur la propagation multi-distance (holotomographie). Jusqu'à présent, les étapes d'estimation de phase et de reconstruction tomographique étaient traitées indépendamment. Ici, nous proposons un nouvel algorithme (CTF-SART) qui combine ces deux étapes en une seule. Il utilise d'une part un modèle linéaire du contraste (appelé Fonction de Transfert du Contraste) pour l'estimation de la phase, et d'autre part l'algorithme itératif SART pour la reconstruction tomographique. Nous décrivons le formalisme de la méthode et présentons les premiers résultats sur données simulées.

Abstract – This work presents a new iterative algorithm for synchrotron radiation micro-tomography, using multi-distance propagation-based phase contrast imaging. Up to now, phase retrieval and tomographic reconstruction were processed as two separated problems. Here, we combine these two parts into a single step algorithm (CTF-SART). A linearized version of the contrast model (known as the contrast transfer function, CTF) was used for phase retrieval, and the simultaneous algebraic reconstruction technique (SART) for the tomographic reconstruction. We present the theoretical framework of the method and the first tests on simulated data.

1 Introduction

X-ray micro-tomography (μ CT) is increasingly considered the reference investigation technique in as diverse fields as materials science, palaeontology and bone research. By the use of synchrotron radiation (SR), a powerful technique is achieved: SR- μ CT. The high flux available in SR- μ CT enables very fast imaging (<1 s/tomographic scan), or the option to monochromatise the beam, which gives access to quantitative measurements of the linear attenuation coefficient. The high flux also makes it feasible to use X-ray focusing optics to achieve nanometric resolutions, for example by implementing an X-ray projection microscope [1].

Additionally, since synchrotron insertion devices constitute partially coherent sources, X-ray phase contrast imaging becomes possible. Due to the short wavelength of X-rays, the phase cannot be measured directly but has to be computed from phase contrast images. Several methods to achieve phase contrast with X-rays have been developed. We focus here on the in-line technique (also known as propagation-based imaging and Fresnel diffraction in literature), where phase contrast is achieved by letting the beam propagate in free space after interaction with the object [2] (Fig. 1).

At relatively short propagation distances, in-line phase contrast appears as an edge enhancement effect. This effect is visible in tomograms as well if the raw phase contrast images are used as input to a tomographic reconstruction algorithm [3]. While this can be a useful modality in its own right, the main interest in this type of phase contrast is that a quantitative, albeit non-linear

relationship exists between the 3D complex refractive index distribution in the imaged object and the contrast measured on the detector. This makes it possible to reconstruct the phase shift induced on the X-ray beam by the imaged object [4]. Combined with tomographic imaging and reconstruction, this allows to reconstruct the refractive index distribution in 3D. We call this modality phase tomography. The main advantages of phase tomography is that it offers several orders of magnitude higher sensitivity than standard attenuation-based tomography, and that the real part of the complex refractive index is proportional to the mass density in the sample, which makes phase tomography images particularly attractive as input to mechanical simulation [5]. The main drawbacks of phase tomography is that it requires an additional reconstruction step, that the reconstruction is sensitive to noise in the low spatial frequency range (this is an intrinsic feature since the information transfer from object to contrast is low in the low spatial

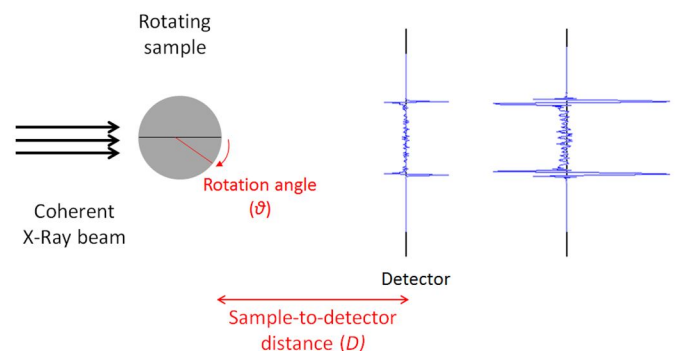


Figure 1 : Schematic of the acquisition geometry in X-ray in-line phase tomography, in 2D

frequency range), and that with the currently available algorithms some spatial resolution is lost [6].

So far, phase tomography has mainly been considered as a two-step process, *i.e.* a 2D phase retrieval step followed by a 3D tomographic reconstruction step. The phase retrieval step has mainly relied on linearization of the contrast model to achieve efficient, filtering-based algorithms. The most well-known linear models include the transport of intensity equation (TIE) [7], the contrast transfer function (CTF) [4], and the mixed approach [8].

Some work has been done on improving the spatial resolution, still in 2D, by considering the full non-linear problem. Langer *et al.* used a non-linear conjugate gradient algorithm to refine an initial reconstruction with a linear algorithm [9]. Davidoiu *et al.* investigated the use of the Frechet derivative to define a Landweber iteration [10], and Moosmann *et al.* used a non-linear filtering-based approach [11].

To address the low-frequency noise sensitivity, different ways to include *a priori* information on the phase have been presented. Paganin *et al.* introduced a homogeneous object assumption by enforcing proportionality between attenuation and phase in the TIE. This yields an algorithm that can retrieve the phase from a single phase contrast image. This can be very useful in practice, despite artefacts where the homogeneity assumption is violated [12]. Langer *et al.* presented a method that assumes homogeneous objects, but where the prior is based on a measurement of the attenuation and is introduced as a regularizing term in a linear least-squares optimization [6].

To reduce the assumptions on the imaged object, some quasi-iterative 3D algorithms have been presented. Beltran *et al.* used reconstructions with Paganin's method at different values of the proportionality constant to achieve an algorithm for multi-material objects. Langer *et al.* introduced an algorithm requiring a reconstructed attenuation tomogram followed by thresholding and forward-projection to achieve an algorithm for multi-material objects [13], and an algorithm that exploits functional relationships between the real and imaginary part of the refractive index for certain materials (e.g. bone) for heterogeneous objects [14].

To further reduce the assumptions on the imaged object, it seems that truly 3D iterative algorithms, that is direct retrieval of the complex refractive index, have to be used. Kostenko *et al.* used Paganin's method combined with a total variation (TV) penalty term in the object domain to achieve an algorithm that albeit still requiring homogeneous objects allows to reduce the number of views acquired in the tomographic scan [15]. Ruhland *et al.* used a Gerchberg-Saxton type algorithm with a consistency constraint to reconstruct the complex refractive index [16]. It is unclear if this algorithm is robust to phase wrapping, however, since it was only demonstrated on weak objects.

In this work, the aim is to combine iterative tomographic reconstruction and phase retrieval to retrieve directly the 3D refractive index distribution,

with the intention to reduce the assumptions on the imaged object by allowing less restrictive priors. To this aim, we present a new algorithm for 3D refractive index retrieval that combines the CTF and the simultaneous algebraic reconstruction technique (SART) [17]. Further, we present the first numerical experiments with this new algorithm on synthetic data, restricted to the 2D case in this initial work.

2 Direct problem

For generality we describe the problem in 3D.

2.1 Image formation

In X-ray phase contrast imaging, we can consider the object fully described by its 3D refractive index distribution

$$n(x, y, z) = 1 - \delta(x, y, z) + i\beta(x, y, z) \quad (0)$$

where the imaginary part is related to attenuation and the real part is related to phase shift. Both attenuation and phase can be considered as straight line projections

$$B(\mathbf{x}) = \frac{2\pi}{\lambda} \int \beta(\mathbf{x}, z) dz \quad (1)$$

$$\varphi(\mathbf{x}) = -\frac{2\pi}{\lambda} \int \delta(\mathbf{x}, z) dz \quad (2)$$

If we consider thin objects, the wave-object interaction can be written as a transmittance function

$$T_\theta(\mathbf{x}) = \exp[-B_\theta(\mathbf{x}) + i\varphi_\theta(\mathbf{x})] \quad (3)$$

which modulates the incident wave so that the exit wave becomes

$$u_{\theta,0}(\mathbf{x}) = T_\theta(\mathbf{x})u_{inc}(\mathbf{x}) \quad (4)$$

Propagation in free space at distance D can be modelled by the Fresnel transform, which can be written as

$$\mathcal{F}r_D = \mathcal{F}^{-1}\tilde{P}_D\mathcal{F} \quad (5)$$

where \mathcal{F} denotes the Fourier transform and $\tilde{P}_D(\mathbf{f})$ is the Fourier transform of the propagator function, given by

$$\tilde{P}_D(\mathbf{f}) = \exp(-i\pi\lambda D|\mathbf{f}|^2) \quad (6)$$

The exit wave can thus be expressed as a linear system with respect to the phase. However, the intensity recorded on the detector, is the intensity of the wave

$$I_{\theta,D}(\mathbf{x}) = |u_{\theta,D}(\mathbf{x})|^2 \quad (7)$$

Hence, the image formation is a non-linear system. The Fourier transform of the intensity can be written as [18]

$$\tilde{I}_D(\mathbf{f}) = \int T\left(\mathbf{x} - \frac{\lambda D\mathbf{f}}{2}\right) T^*\left(\mathbf{x} + \frac{\lambda D\mathbf{f}}{2}\right) \exp(-i2\pi\mathbf{x}\mathbf{f}) d\mathbf{x} \quad (8)$$

2.2 Contrast Transfer Function

The contrast transfer function model is derived by Taylor expanding both the attenuation and phase terms in the transmittance function to the first order

$$T(\mathbf{x}) \approx 1 - B(\mathbf{x}) + i\varphi(\mathbf{x}) \quad (9).$$

It can be shown that this linearization is valid if the attenuation is weak and the phase is slowly varying, *i.e.*

$$B(\mathbf{x}) \ll 1 \quad (10)$$

and

$$|\varphi(\mathbf{x}) - \varphi(\mathbf{x} + \lambda D \mathbf{f})| \ll 1 \quad (11).$$

Substituting Eq. (9) into Eq. (8) yields

$$\tilde{I}_D(\mathbf{f}) = \delta_{Dirac}(\mathbf{f}) - 2 \cos(\pi \lambda D |\mathbf{f}|^2) \tilde{B}(\mathbf{f}) + 2 \sin(\pi \lambda D |\mathbf{f}|^2) \tilde{\varphi}(\mathbf{f}) \quad (12)$$

which is the contrast transfer function. This model can be used to solve for both phase and attenuation using linear least-squares optimization (denoted LSQ in this paper). Here, we consider only the pure phase case, which means that the cosine term disappears. The solution for the phase becomes

$$\tilde{\varphi}(\mathbf{f}) = \frac{\sum_{D=1}^N \sin(\pi \lambda D |\mathbf{f}|^2) [\tilde{I}_D(\mathbf{f}) - \delta_{Dirac}(\mathbf{f})]}{[\sum_{D=1}^N 2 \sin^2(\pi \lambda D |\mathbf{f}|^2)] + \alpha} \quad (13)$$

where α is an arbitrary regularization parameter [4].

2.3 Simultaneous Algebraic Reconstruction Technique (SART)

The tomographic reconstruction problem can be expressed as:

$$\mathbf{p} = \mathcal{R} \mathbf{f} \quad (14)$$

where \mathbf{p} represents the measurements (*e.g.* the projections), \mathbf{f} the unknown (*e.g.* the attenuation map) and \mathcal{R} the transformation (*e.g.* the Radon transform). Conversely to the conventional filtered back-projection (FBP) algorithm, iterative solutions are increasingly used. These methods enable to solve linear problems, that requires a first estimate of the unknown \mathbf{f} , $\mathbf{f}^{(0)}$. Here, we consider the SART algorithm. At the k^{th} iteration, $\mathbf{f}^{(k)}$ is estimated from the difference between $\mathcal{R}_\vartheta \mathbf{f}^{(k-1)}$ and the measurement at angle ϑ , \mathbf{p}_ϑ , using the following formula [17]:

$$\mathbf{f}^{(k)} = \mathbf{f}^{(k-1)} + \mathcal{R}_\vartheta^T \frac{\mathbf{p}_\vartheta - \mathcal{R}_\vartheta \mathbf{f}^{(k-1)}}{\|\mathcal{R}_\vartheta\|^2} \quad (15)$$

3 Proposed reconstruction algorithm

Here, we combine CTF and SART to achieve a refractive index retrieval algorithm. We start by expressing the Fourier transform of the intensity as a function of the refractive index decrement, for a pure phase object

$$\tilde{I}_{D,\vartheta}(\mathbf{f}) = \delta_{Dirac}(\mathbf{f}) + 2 \sin(\pi \lambda D |\mathbf{f}|^2) \mathcal{F} \left[-\frac{2\pi}{\lambda} \mathcal{R}_\vartheta \delta \right](\mathbf{f}) \quad (16)$$

where \mathcal{R}_ϑ is the projection operator at angle ϑ . The object is non absorbing, thus the hypothesis (10) is verified.

For simplicity, we rewrite this as

$$\tilde{I}_D(\mathbf{f}) = \delta_{Dirac}(\mathbf{f}) + A_D(\mathbf{f}) \mathcal{F}[\mathcal{R}_\vartheta \delta](\mathbf{f}) \quad (17)$$

The contrast can then be written in the spatial domain as

$$I_D(\mathbf{x}) = \mathcal{F}^{-1}\{A_D \mathcal{F}[\mathcal{R}_\vartheta \delta]\}(\mathbf{x}) + 1 \quad (18)$$

Substituting the contrast operator in Eq. (12) for \mathcal{R} in the SART formula (Eq. 15) yields the following iteration formula

$$\begin{aligned} \delta^{(k)}(\mathbf{x}) &= \delta^{(k-1)}(\mathbf{x}) \\ &+ \mathcal{R}_\vartheta^T \frac{\mathcal{F}^{-1}\{A_D \tilde{I}_D\}(\mathbf{x}) - \mathcal{F}^{-1}\{A_D^2 \mathcal{F}\{\mathcal{R}_\vartheta \delta^{(k-1)}\}\}(\mathbf{x}) - 1}{\|\mathcal{F}^{-1}\{A_D(\mathbf{f}) \mathcal{F}[\mathcal{R}_\vartheta]\}\|^2} \end{aligned} \quad (19)$$

3.1 Implementation

In these initial numerical experiments we limit ourselves to the 2D reconstruction of pure phase objects from multi-distance acquisitions. \mathcal{R}_ϑ and \mathcal{R}_ϑ^T are implemented using `radon()` and `iradon()` in Matlab. $\|A_D(\mathbf{f})\|$ is a constant dependent on D and can be pre-calculated. Here, $\|\mathcal{R}_\vartheta\|$ is approximated by the path length of the rays, which can also be pre-calculated using `radon()`. In each cycle, a distance is chosen randomly, and all projection angles are traversed in random order for that distance. This is repeated until all distances are taken into account. A preliminary study actually showed that 20 cycles is a good trade-off between convergence and computation time.

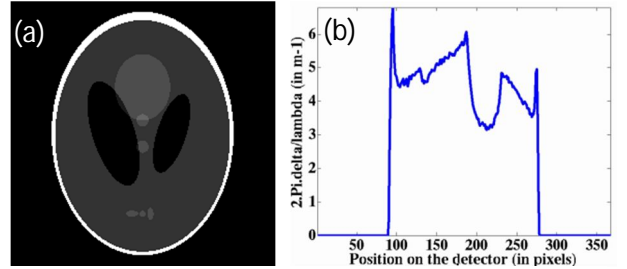


Figure 2 : (a) Original object, a modified Shepp-Logan phantom, and (b) a phase projection. Note that the phase exceeds 2π

4 Numerical experiments

Numerical experiments were performed using a modified 2D Shepp-Logan phantom. The image range was adjusted to yield phase projections that exceed 2π . The image size was 256×256 pixels (Fig. 2). Intensities at different distances were simulated using the squared modulus of the Fresnel transform. The X-ray energy used for these simulations was 19 keV and the pixel size was $3.5 \mu\text{m}$, which corresponds to common experimental conditions. Based on these conditions, the four following propagation distances were chosen according to Zabler *et al.* [19]: $D=[0.303; 0.636; 1.635; 1.968]$ m. Fig 3 illustrates the two simulated sinograms at the first and fourth distances. Detection was simulated by adding noise so that the Peak-to-Peak Signal to Noise Ratio (PPSNR) is equal to 48 dB in the simulated intensities. Fig 4 shows the reconstructed images both with CTF-ART and LSQ for the noise-free and noisy data.

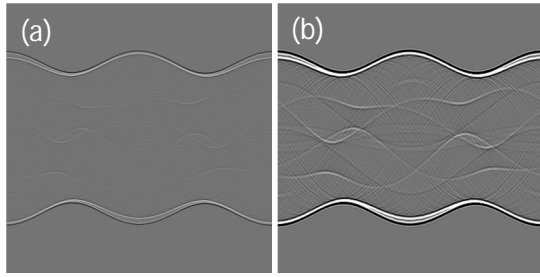


Figure 3 : Simulated sinograms for the modified Shepp-Logan phantom at (a) $D=0.303\text{m}$ (b) $D=1.968\text{m}$.

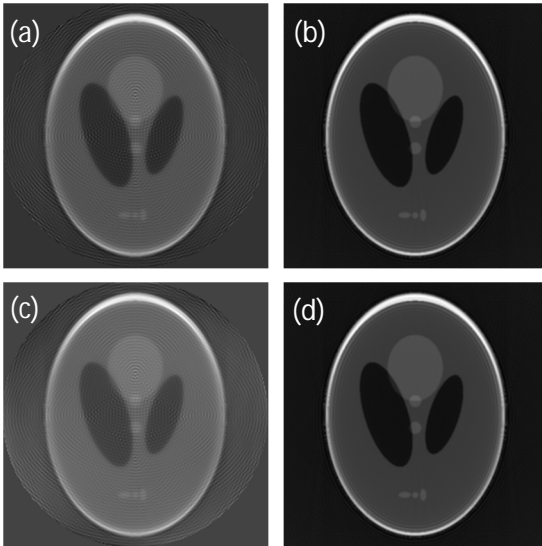


Figure 4 : Reconstructed images data without noise using (a) CTF-SART and (b) LSQ method, and from noisy data (PPSNR=48 dB) using (c) CTF-SART and (d) LSQ method.

5 Discussion and conclusions

Regarding reconstructed images (Fig. 4), CTF-SART yields promising results. The qualitative features of the object are clearly visible, but the LSQ leads to sharper and more quantitative reconstructed images. For example, the reconstructed image from noisy data contains a varying background (low- frequency noise). The LSQ incorporates Tikhonov-like regularization in the projections domain, however. There are some little fringes remaining with both reconstruction methods. This is probably due to an insufficient oversampling for the Fresnel transform.

In this paper, we present the very first tests for an innovative algorithm that combines phase retrieval and tomographic reconstruction. While the initial results are promising, further refinement of the implementation of CTF-SART is needed. We plan to extend this algorithm to objects including both phase and attenuation which increases the dimensionality of the problem. The final goal would be to be able to reconstructed phase and attenuation without having to measure an attenuation image, which increase the ill-posedness of the problem. The advantage of this combined phase-tomographic reconstruction approach is that it will also be possible to add a regularization term in the object domain. Further, we could introduce different regularization for attenuation and phase, and retrieve these entangled quantities alternatively.

6 Acknowledgments

This work was supported by the LABEX PRIMES (ANR-11-LABX-0063) of Université de Lyon, within the program "Investissements d'Avenir" (ANR-11-IDEX-0007) operated by the French National Research Agency (ANR).

7 References

- [1] R. Mokso, P. Cloetens, E. Maire, W. Ludwig, and J.-Y. Buffière, *Appl. Phys. Lett.* **90**, 144104, 2007.
- [2] A. Snigirev, I. Snigireva, V. Kohn, S. Kuznetsov, and I. Schelokov, *Rev. Sci. Instrum.* **66**, 5486, 1995.
- [3] P. Cloetens, M. Pateyron-Salomé, J. Y. Buffière, G. Peix, J. Baruchel, F. Peyrin, and M. Schlenker, *J. Appl. Phys.* **81**, 5878, 1997.
- [4] P. Cloetens, W. Ludwig, J. Baruchel, D. Van Dyck, J. Van Landuyt, J. P. Guigay, and M. Schlenker, *Appl. Phys. Lett.* **75**, 2912, 1999.
- [5] P. Varga, B. Hesse, M. Langer, S. Schrof, N. Männicke, H. Suhonen, A. Pacureanu, D. Pahr, F. Peyrin, and K. Raum, *Biomech. Model. Mechanobiol.* **14**, 267–282, 2015.
- [6] M. Langer, P. Cloetens, and F. Peyrin, *IEEE Trans. Image Process.* **19**, 2428–2436, 2010.
- [7] K. Nugent, T. Gureyev, D. Cookson, D. Paganin, and Z. Barnea, *Phys. Rev. Lett.* **77**, pp. 2961–2964, 1996.
- [8] M. Langer, P. Cloetens, J. P. Guigay, S. Valton, and F. Peyrin, *IEEE International Symposium on Biomedical Imaging (ISBI)*, 552–555, 2007.
- [9] M. Langer, A. Pacureanu, H. Suhonen, Q. Grimal, P. Cloetens, and F. Peyrin, *Plos one* **7**, e35691, 2012.
- [10] V. Davidoiu, B. Sixou, M. Langer, and F. Peyrin, *Opt. Express* **19**, 106–109, 2011.
- [11] J. Moosmann, R. Hofmann, A. Bronnikov, and T. Baumbach, *Opt. Express* **18**, 25771–25785, 2010.
- [12] D. Paganin, S. C. Mayo, T. E. Gureyev, P. R. Miller, and S. W. Wilkins, *J. Microsc.* **206**, 33–40, 2002.
- [13] M. Langer, P. Cloetens, A. Pacureanu, and F. Peyrin, *Opt. Lett.* **37**, 2151–2153, 2012.
- [14] M. Langer, B. Hesse, A. Pacureanu, H. Suhonen, P. Cloetens, K. Raum, and F. Peyrin, *Phil. Trans. R. Soc. A* **372**, 20130129, 2013.
- [15] A. Kostenko, K. J. Batenburg, H. Suhonen, S. E. Offerman, and L. J. van Vliet, *Opt. Express* **21**, 710–723, 2013.
- [16] A. Ruhlandt, M. Krenkel, M. Bartels, and T. Salditt, *Phys. Rev. A* **89**, 033847, 2014.
- [17] A. H. Andersen and A. C. Kak, *Ultrason. Imaging* **6**, 81–94, 1984.
- [18] J.-P. Guigay, *Optik* **49**, 121–125, 1977.
- [19] S. Zabler, P. Cloetens, J.-P. Guigay, J. Baruchel, and M. Schlenker, *Rev. Sci. Instrum.* **76**, 073705, 2005.